JACS
JOURNAL OF THE AMERICAN CHEMICAL SOCIETY

ARTICLE

pubs.acs.org/JACS

Theoretical Procedure for Optimizing Dye-Sensitized Solar Cells: From Electronic Structure to Photovoltaic Efficiency

Tangui Le Bahers,[†] Frédéric Labat,[†] Thierry Pauporté,[*,†] Philippe P. Lainé,[*,‡] and Ilaria Ciofini[*,†]

[†]Laboratoire d'Electrochimie, Chimie des Interfaces et Modélisation pour l'Energie, UMR 7575 CNRS, Ecole Nationale Supérieure de Chimie de Paris—Chimie ParisTech, 11 rue P. et M. Curie, 75231 Paris Cedex 05, France

[‡] Laboratoire ITODYS, UMR 7086 CNRS, Université Paris Diderot, Sorbonne Paris Cité, Bâtiment Lavoisier, 15 rue Jean Antoine de Baïf, 75205 Paris Cedex 13, France

Supporting Information

ABSTRACT: A step-by-step theoretical protocol based on density functional theory (DFT) and time-dependent DFT at both the molecular and periodic levels is proposed for the design of dye-sensitized solar cell (DSSC) devices including dyes and electrolyte additives. This computational tool is tested with a fused polycyclic pyridinium derivative as a novel dye prototype. First, the UV−vis spectrum of this dye alone is computed, and then the electronic structure of the system with the dye adsorbed on an oxide semiconductor surface is evaluated. The influence of the electrolyte part of the DSSC is investigated by explicitly taking into account the electrolyte molecules co-adsorbed with the dye on the surface. We find that *tert*-butylpyridine (TBP) reduces the electron injection by a factor of 2, while lithium ion increases this injection by a factor of 2.4. Our stepwise protocol is successfully validated by experimental measurements, which establish that TBP divides the electronic injection by 1.6 whereas Li^+ multiplies this injection by 1.8. This procedure should be useful for molecular engineering in the field of DSSCs, not only as a complement to experimental approaches but also for improving them in terms of time and resource consumption.

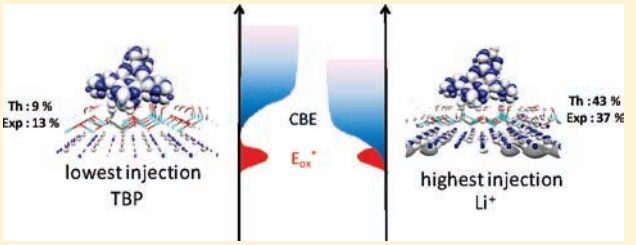

INTRODUCTION

Dye-sensitized solar cells (DSSCs) have attracted a considerable amount of attention since O'Regan and Grätzel published their pioneering work in 1991.[1,2] Due to their low costs, these devices appear to be a good alternative to silicon-based solar cells. Intensive research has been performed in order to increase the photoconversion efficiency, reaching values higher than 10% for titania-based DSSCs sensitized with ruthenium complexes (e.g., N719)[3,4] and organic dyes.[5] Different approaches for improving DSSCs are still being explored. The nature of the semiconductor (TiO_2,[3] SnO_2,[6] ZnO,[7] NiO,[8] etc.) and its morphology (TiO_2,[3,9,10] ZnO,[11,12] etc.) are both important parameters that can be modified. The dye is also adaptable as well as the electrolyte composition. Every combination of these parameters should be tested in order to identify the best DSSC setup. However, not only because the number of such combinations is very large, but also due to the complex (multi)functional nature of DSSC devices, a fully combinatorial approach is not workable.

In this study, a theoretical protocol is proposed with the aim of assisting researchers working in the field of photovoltaics in the well-educated choice of both the dyes and the electrolyte composition for DSSC applications. The main idea behind this computational modeling is to determine qualitatively, or even quantitatively, whether or not a certain type of semiconductor/dye/electrolyte system will be able to efficiently generate a photocurrent. One could thus avoid embarking in a time- and resources-consuming synthesis and fabrication process that could lead to a loosely operational system.

The case study selected to illustrate the relevance of our computational approach is the optimization of a ZnO-based DSSC device. The first element of a novel pyridinium-based family of dyes—hereafter referred to as P1 (Figure 1)—was chosen as a prototypical sensitizer not only because its suitability to fulfill this function in a DSSC was hitherto unknown but also because pyridinium derivatives in general are rarely meant for this use.[13] This push−pull organic photosensitizer results from the covalent assembly of (i) a so-called expanded pyridinium (that is, a pyridinium core embedded within the π-extended system of a fused polycyclic fragment)[14−16] as the electron-withdrawing component, (ii) a *p*-aminophenyl moiety as the electron-releasing component, and (iii) a carboxylate group, which is known for strongly chemisorbing on oxide surfaces.[17−19] As the targeted semiconductor is ZnO, the anchoring group is most likely in its deprotonated form since ZnO is very sensitive to acidic media.[20] Of note, the spatially well-defined donor−acceptor−anchoring group directional layout of components is an important functional template for dyes employed in DSSC devices.[21]

Received: March 3, 2011
Published: April 22, 2011

dx.doi.org/10.1021/ja201944g | *J. Am. Chem. Soc.* 2011, 133, 8005–8013

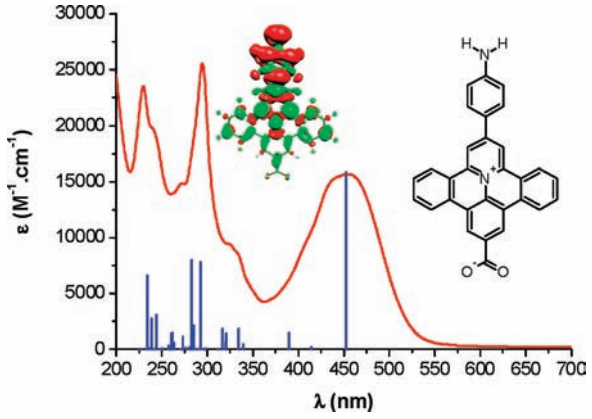

Figure 1. Superimposed experimental UV−vis spectrum measured in ethanol (red) and computed electronic transitions (TD-DFT/PBE0/6-31++G(d,p), blue) along with the molecular structure of P1 and the computed difference in electronic density between the first excited state and the ground state (green and red refer to an increase and a decrease of electronic density, respectively; isovalue 0.0005 au).

Computations are performed using the density functional theory (DFT) and its time-dependent extension (TD-DFT) at both the molecular and periodic levels. Indeed, it is recognized that DFT can reproduce accurately geometric and electronic structures of molecules as well as hybrid interfaces.[17,21−24]

The paper is structured as follows. After a description of computational and experimental setups, the results are presented in two sections. The first accounts for the stepwise theoretical procedure we applied through the discussion of the following items: (1) Determination of intrinsic features of the dye by computing structural and electronic properties of the isolated species. (2) Assessment of the impact of adsorption on the P1 dye's features by determining the electronic structure of the system comprised of the dye molecule and the semiconductor. (3) Evaluation of the influence of electrolyte on the electronic structure of the dye/semiconductor systems. To this end, explicit electrolyte molecules are co-adsorbed on the surface in the vicinity of the dye. An estimate of the electron injection efficiency is given for each analyzed case.

In the second section, these computational outcomes are compared and validated by current−potential characteristics (noted $J-V$) and incident photon-to-electron conversion efficiency (IPCE) measurements performed on P1/ZnO DSSCs. Theoretical predictions allowed optimizing the electrolyte composition, thereby improving the overall cell efficiency by 30%.

The last section summarizes the theoretical protocol we perfected and generalizes the implementation of this procedure to various possible oxide/dye/electrolyte combinations.

THEORETICAL SETUP

Molecular calculations were carried out with the Gaussian09 code.[25] A hybrid Hartree−Fock/density functional model, referred to as PBE0, was used.[26] This functional was chosen as it has recently been proven to yield reliable valence excitations in organic dyes and, provided that a sufficient orbital overlap is present, also excitation with charge transfer character.[15,16,21,24]

Structural optimizations and subsequent frequency calculations for the ground state were performed using an all-electron Pople double-ζ basis set with one polarization function on heavier atoms (6-31+G(d)).[27] Vertical excitations were computed by the means of TD-DFT at the same level of theory, adding diffuse and polarization functions on hydrogen atoms (6-31++G(d,p) basis[27]). Bulk solvent effects were included using the polarizable continuum model (PCM) of Tomasi and co-workers.[28] More specifically, the conductor-like PCM model as implemented in Gaussian (CPCM)[29] was applied, and ethanol was considered as solvent in analogy with the experimental medium. Default radii (from the UFF, scaled by 1.1) were used for structural optimizations.

Periodic calculations were carried out with the *ab initio* CRYSTAL09 code,[30] making use of localized (Gaussian) basis sets and solving self-consistently Hartree−Fock and Kohn−Sham equations, thus allowing the efficient use of hybrid functionals for band structure calculations.

The most stable crystallographic surface of the wurzite phase of ZnO (that is, the {100} plane) was considered for the adsorption of the dye and additive molecules since this surface is the predominant one for solution-grown ZnO nanostructures.[31] Two-dimensional periodic slab models were taken into account in order to model adsorption, the unit cell being defined by two lattice parameters a and b along the ⟨120⟩ and ⟨001⟩ directions, respectively.

Water and dye adsorptions were investigated making use of rectangular (2×1) and (6×4) supercells, respectively. Sampling of the irreductible brillouin zone was done with 9 k-points for the (2×1) supercell and 1 k-point for the (6×4) supercell.

An all-electron basis set with 7-311G(d), 8-411G(d), 6-21G(d), 511G(p), and 5-11G(d) contractions for N, O, C, H, and Li atoms described the dye, MP, and Li adsorbates.[32] Durand and Barthelat large-core pseudopotentials with (31/31)[33,34] contractions were used for O atoms of the ZnO substrate and water molecules, while large-core Hay and Wadt pseudopotentials with (111/111/41) contractions were considered for Zn atoms[35] and the 31G(p) all-electron basis set for the H atoms of water molecules.[32]

Periodic calculations were performed at the DFT level, applying the hybrid exchange correlation functional PBE0 previously used for molecular calculations. This level of theory has already proven to provide reliable geometrical and electronic properties of molecules and periodic systems.[17,19,36]

A detailed description of the procedure of optimization of water molecules on the ZnO surface and determination of cell parameters is given in the Supporting Information. The so-optimized surface was next used to obtain the (6×4) supercell with the withdrawal of two water molecules in order to allow dye adsorption.

During the dye adsorption (with or without additives), all the adsorbed molecules (dye, water, and additives) were allowed to fully relax as the two outermost atomic planes, since surface relaxation of this substrate is known to mainly involve only the outermost planes.[17] The cell parameters a and b were taken from the water adsorption and were not allowed to relax further.

EXPERIMENTAL SETUP

The synthesis of the molecule P1 was carried out following adaptations of literature procedures perfected for affiliated fused expanded pyridiniums[14,16,37] and will be reported elsewhere (see also the Supporting Information).

The nanoporous ZnO substrate was obtained by a procedure detailed in refs 7, 11, 19, 38, and 39.

Before dye adsorption, the ZnO sample was dried at 150 °C for 1 h. It was then immersed overnight in a 0.5 mM solution of P1 in ethanol at room temperature. Cholic acid was co-adsorbed by adding a 1 mM concentration of this molecule in the dye solution.

The cells were built by assembling the photoanode (i.e., the zinc oxide sensitized by P1) and a counter electrode (a platinized FTO-glass substrate). The illuminated area was fixed at 0.20 cm^2. Three electrolytes are tested in the present publication. The standard one (without

additives) contained 0.6 M tetrabutylamonium iodide and 0.05 M iodine in acetonitrile. The electrolyte containing lithium ion was made of 0.3 M tetrabutylamonium iodide, 0.3 M lithium iodide, and 0.05 M iodine in acetonitrile. The electrolyte containing *tert*-butylpyridine (TBP) was similar to the standard one but with addition of 0.5 M TBP. The photovoltaic performances of the devices were recorded under 100 mW/cm^2 simulated AM1.5 solar light illumination immediately after cell assembly. The IPCE spectra were recorded with a home-made Jobin-Yvon spectral system.

RESULTS AND DISCUSSION

Computational Protocol. *1. Intrinsic Properties of the Dye P1.* In order to be suitable for DSSCs applications, dyes must show some intrinsic properties such as (i) a large electronic absorptivity in the visible region and (ii) a preferably donor−acceptor−anchoring group directional structure. The UV−vis absorption spectrum of P1 molecule in ethanol was computed at the TD-DFT level, of proven accuracy for the determination of the electronic properties of organic dyes.[21,24] In order to take into account direct solute−solvent interactions, two ethanol molecules were placed near the amino group. Optimized structural parameters computed for this system are reported in the Supporting Information (Figure S3 and Table S1). The effect of addition of supplementary ethanol molecules near the acceptor has also been considered but was found to be negligible (Supporting Information, Figure S4). As expected, these values are very close to those previously reported for similar molecules of this family.[14,40] Computed absorption energies and corresponding oscillator strengths are depicted in Figure 1. The first transition (corresponding to a HOMO−LUMO excitation) is calculated at 453 nm, with an oscillator strength of 1.05, thus predicting a strong absorption in the visible region. To establish the nature of this transition, the variation of the total electronic density between the ground state and the first excited state is also reported in Figure 1. Clearly, this transition shows a strong charge-transfer character: upon light absorption, the electronic density is depleted on the aminophenyl group and increased on the pyridinium ring. This observation is in agreement with the respective electron-donating and -accepting properties of the aminophenyl and pyridinium groups, as suggested above. The computed increase of the dipole moment vertically on going from the ground to the excited state of +13.6 D further confirms the charge-transfer character of this transition. Interestingly, the calculated enhancement of dipole moment is of the same order of magnitude as those computed for dyes of the indoline family.[21] Of note, the anchoring group is practically not involved in this electronic transition. Moreover, the energy of the LUMO of P1 is calculated to be 0.2 eV above the conduction band edge of a bare ZnO surface, as found for indoline dyes in ref 21. Thus, on the basis of this molecular approach, the P1 molecule should be efficient for DSSC applications.

2. Interaction between the Dye and the Semiconductor Surface. To better account for the functioning of the system, the interaction between the dye and the surface was investigated using DFT-based methods with periodic boundary conditions. The surface studied is the {100} surface of the wurtzite structure of ZnO, which is the predominant surface for electrodeposited ZnO.[12,41] Passivation of the surface was simulated by adsorption of water molecules. Indeed, in the real device, the surface is in contact with different solvents (whether originating from the dye or the electrolyte solutions). Consequently, a mixture of different types of passivating solvent molecules most likely covers the surface. In our model, various types of solvent molecules were replaced by water in order to decrease the computational burden. The influence of water molecules on the electronic structure of the ZnO surface was investigated first (see the Supporting Information). Since all electronic parameters (such as density of states (DOS), conduction band (CB), and valence band (VB) edge positions) were found to remain practically identical to those calculated for a bare ZnO surface, we consider that this method is relevant for simulating passivation without introducing artifacts. The same assumption was made previously by De Angelis et al. in the case of ZnO clusters.[42] The dye was adsorbed via its carboxylate group in a bridged-bidentate manner, which has been proved to be the most stable adsorption mode for this anchoring group.[17,19] The final geometry is presented in Figure 2a, while detailed geometrical parameters are given in the Supporting Information (Table S1). No significant changes upon adsorption are computed with regard to internal geometrical parameters of the molecule, revealing the overall rigidity of the backbone of this dye. Only the dihedral angle $\theta 1$ (corresponding to the tilt angle between the pyridinium ring and the coplanar aminophenyl fragment) changes upon adsorption. This angle is actually known to be very sensitive to the environment.[40] The P1 molecule leans in the direction $\langle 00{-}1 \rangle$, with a tilt angle of ca. 35° with respect to the surface plane. The Zn−O distances (2.071 and 2.032 Å) are very similar to the computed Zn−O distances in the cases of adsorptions of both esosin Y (2.067 and 2.016 Å)[36] and simple formate (2.038 and 2.008 Å)[17] on the ZnO {100} surface, confirming the strong chemisorption of the dye. With regard to electronic features, computing the DOS of this system (see Figure 3a) is also very informative. For DSSCs to work efficiently, at least two electronic requirements must be fulfilled: (i) the HOMO of the dye must lie in the bandgap of the semiconductor, and (ii) the LUMO of the dye must lie right above the CB bottom edge of the semiconductor. In our case (P1), the HOMO and the LUMO of the dye lie below the VB and CB edges of the semiconductor, respectively. In particular, the calculated energy difference between the CB bottom edge of ZnO and the LUMO of P1 is ca. 0.58 eV, which is different from the configuration derived from molecular calculations (see above). This gap is actually overestimated for two reasons: (i) the real oxidative potential of the excited dye is not related to a single level but rather to a sharp band resulting from the distribution of environments around the dye,[2] and (ii) the entropy contribution from the defects in the ZnO (involved in the electron diffusion in the film) is not included in the CB edge calculation. This factor is known to be very large[2] and lowers the energy of the CB bottom edge. For these reasons, even if the LUMO is computed to lie ca. 0.58 eV below the CB bottom edge, there could exist in the real device a non-negligible overlap between the LUMO and the CB edge that may permit electron injection. Nevertheless, with such an orbital configuration, the injection rate is anticipated to be low, as confirmed experimentally (see below).

In summary, contrary to the molecular approach used for studying the properties of the isolated dye, only the periodic calculations explicitly integrating both the ZnO surface and the dye allow us to predict (and show) that ZnO sensitized by P1 should have a low efficiency due to the unfavorable electronic structure for electron injection.

3. Effects of Electrolyte Interactions. The choice of the electrolyte is a greatly adjustable parameter for optimizing DSSCs' efficiency because the electrolyte component is usually made of

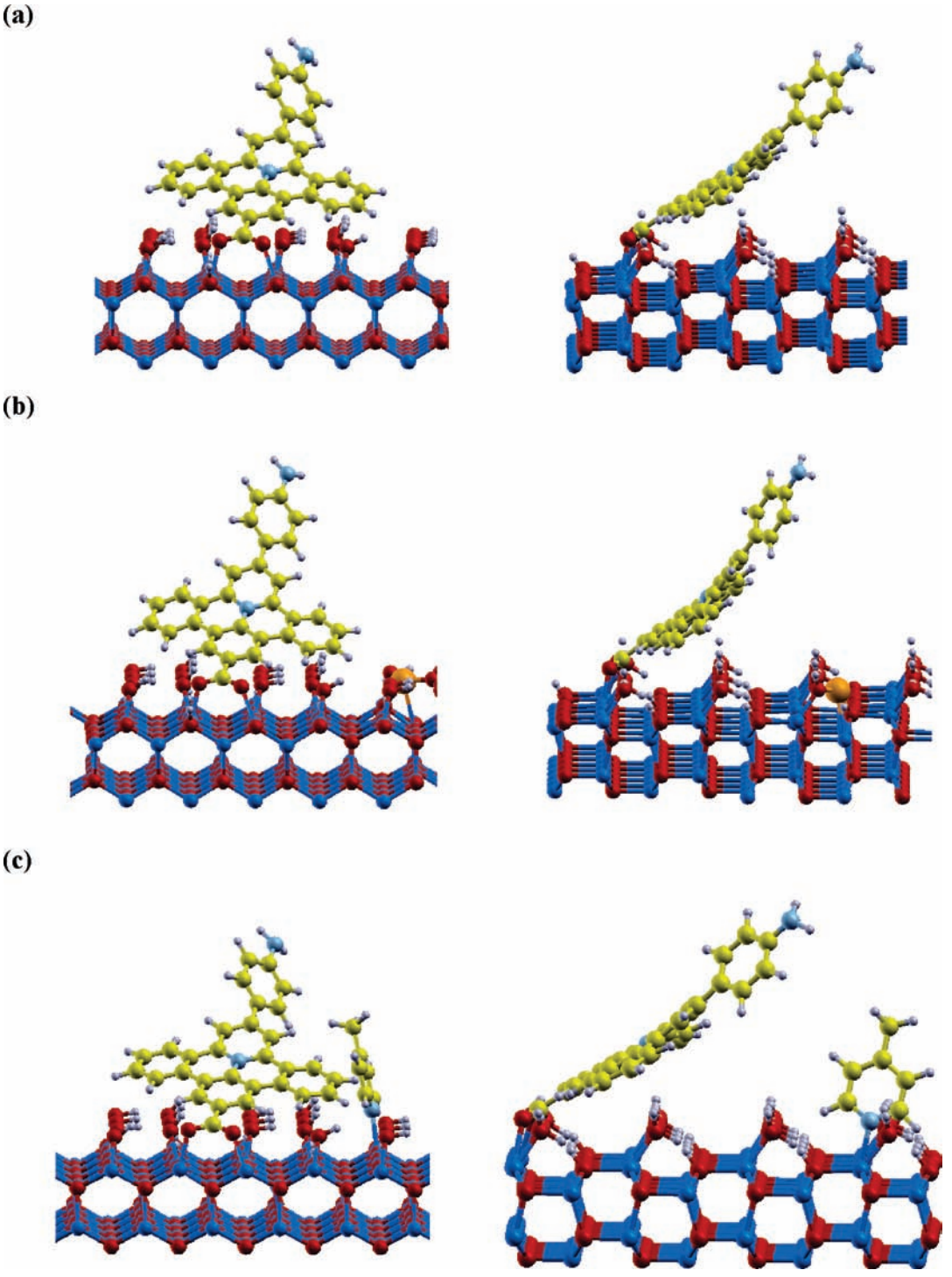

Figure 2. Optimized structure of passivated P1/ZnO (a), (P1+Li^+)/ZnO (b), and (P1+TBP)/ZnO (c) systems. The color scheme adopted is blue, red, yellow, sky blue, gray, and orange for Zn, O, C, N, H, and Li atoms, respectively.

several tunable types of molecules. Indeed, it contains iodine (in the tri-iodide form), iodide ions (with a counterion), solvent, and various additives (for "boosting" the efficiency, in particular, by properly modifying the energy of the CB bottom edge).[23] In fact, both solvent and additives can affect the CB edge by adsorbing on the oxide surface and, consequently, modify the DSSC's efficiency. For instance, molecules with large numbers of donors (such as TBP) are known to increase the energy of the CB bottom edge.[23] Conversely, lithium ion (Li^+) or guanidinium thiocyanate is commonly used to decrease the energy of the CB bottom edge.[43,44]

Using the periodic approach developed in section 2 to model the interaction between the surface of ZnO and the dye P1, explicit additive molecules were co-adsorbed with the dye on a water-passivated ZnO surface. In particular, we focused on the influences of two different additives, having opposite impacts on

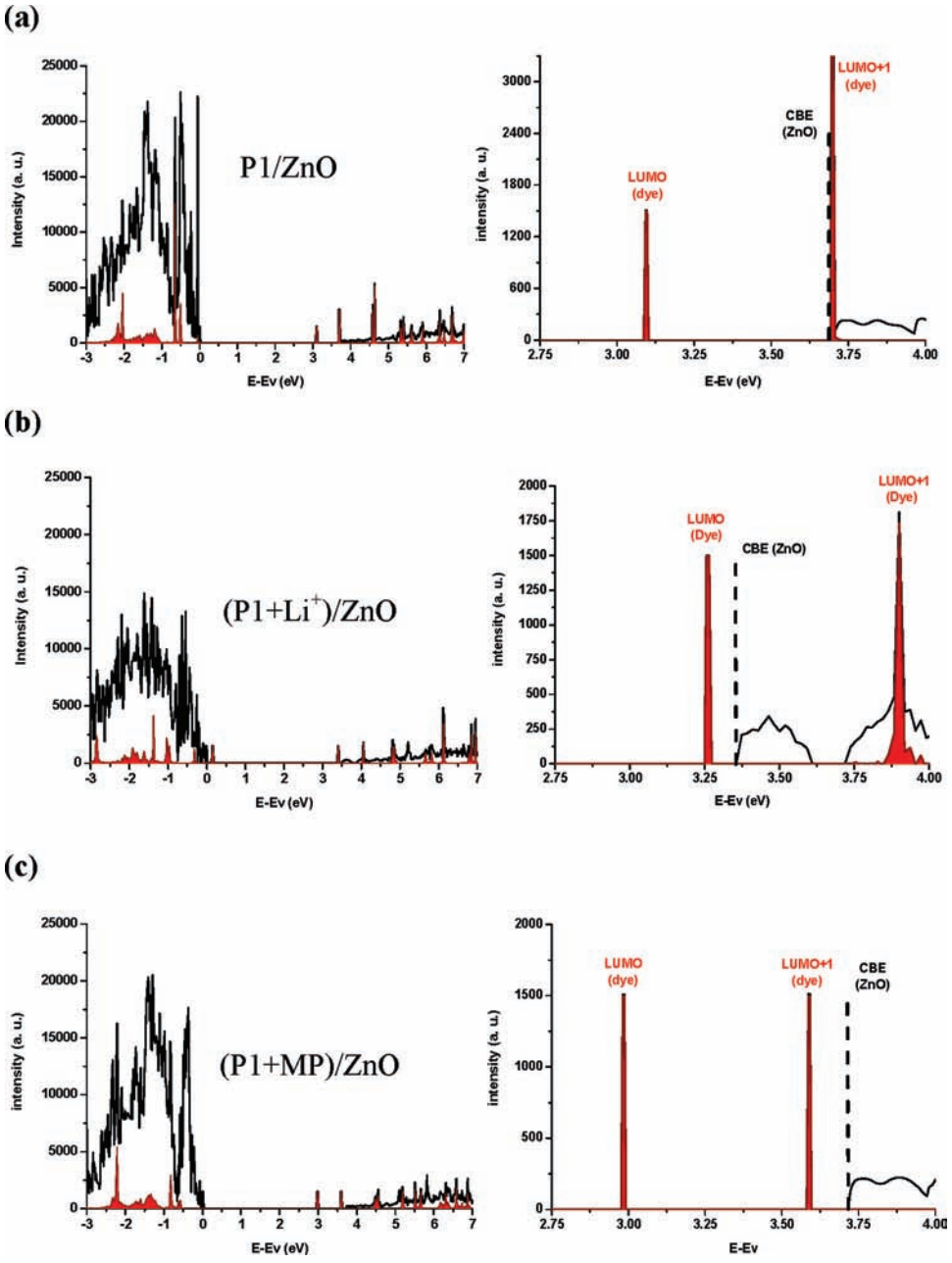

Figure 3. Density of states of P1 adsorbed on a ZnO {100} surface (right) and zoom-in of the CB edge region (left) computed for the P1/ZnO (a), (P1+Li^+)/ZnO (b), and (P1+MP)/ZnO (c) systems. The color scheme adopted is black for the total DOS of the system and red for the DOS projected on the P1 molecule.

the bottom edge of the CB of the oxide-based semiconductor, namely Li^+ (reducing the open-circuit voltage, V_{oc})[44,45] and TBP (leading to higher V_{oc}).[23] In the present work, TBP is modeled by 4-methylpyridine (noted MP) to reduce the computational burden. This simplification was successfully validated in a previous work.[23] Optimized structures of these systems are depicted in Figure 2b,c, and corresponding geometrical parameters are collected in Table S1. The structure of the adsorbed dye (P1) is barely affected by the presence of co-adsorbed additive molecules. As expected, the Li^+ cation interacts with an oxygen atom of the surface, with a Li−O distance of 1.809 Å, while the MP molecule preferably adsorbs on a Zn atom, with a N−Zn distance of 2.123 Å.

The DOS patterns of the (P1+Li^+)/ZnO and (P1+MP)/ZnO systems are presented in Figure 3b,c. In the case of the co-adsorbed MP molecule, the electronic structure of the system is very similar to the one obtained for P1 adsorbed on a water-passivated ZnO surface, presented above (i.e., HOMO and LUMO levels lying below the VB and CB critical edges of ZnO, respectively). With the Li^+ additive, a significant variation is observed since the HOMO of P1 no longer lies below the VB top edge of ZnO but is instead located 0.14 eV above it. Interestingly, even if the LUMO of this system remains below the CB bottom edge, adsorption of Li^+ sizably decreases the gap between the LUMO and the CB edge by ca. 0.45 eV (from 0.58 to 0.12 eV). Contrary to Li^+, the MP molecule increases this

dx.doi.org/10.1021/ja201944g |*J. Am. Chem. Soc.* 2011, 133, 8005–8013

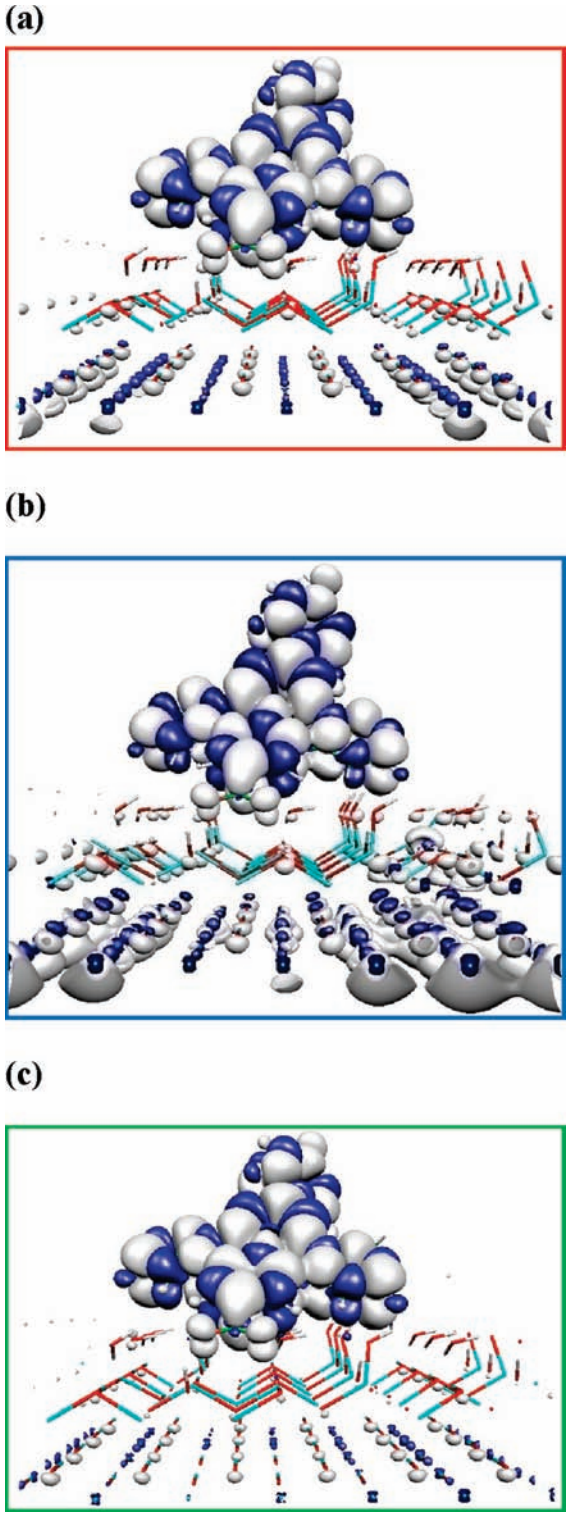

Figure 4. Spin densities of reduced P1/ZnO (a), (P1+Li^+)/ZnO (b), and (P1+MP)/ZnO (c) systems (isocontour value 0.0001 au).

energy gap from 0.58 to 0.74 eV. These calculations confirm the abilities of Li^+ and MP (and, by analogy, of TBP) to change the energy of the critical CB bottom edge of oxides and clearly predict that these additive molecules should substantially influence the electron injection in the case of the P1/ZnO system. More precisely, addition of Li^+ is anticipated to improve the energy matching of the LUMO of the dye and the bottom edge of the CB, thereby enhancing the efficiency of electron injection. For the same reasons, the presence of TBP should result in a reduced rate of electron injection.

Table 1. Measured and Computed Properties of P1/ZnO Systems in the Absence or Presence of Cholic Acid, in the Presence of Lithium Ion or TBP in the Electrolyte[a]

additives	V_{oc}	J_{sc}	FF	η	IPCE	α spin excess	CBE-LUMO
none	0.50	1.3	73	0.5	17	–	–
cholic acid	0.51	1.8	67	0.6	21	18	0.58
cholic acid/Li^+	0.43	3.3	62	0.9	37	43	0.12
cholic acid/TBP	0.49	1.1	72	0.4	13	9	0.74

[a] V_{oc} (open-circuit voltage, V), J_{sc} (short-circuit current, mA/cm^2), FF (fill factor, %), and η (power conversion efficiency, %) are from $J-V$ measurements under AM1.5. IPCE values (%) are the maximum values of the measured IPCE spectra. α spin excess (%) represents the computed proportion of injected electrons in ZnO. CBE-LUMO (eV) is the computed gap between the dye's LUMO and the CB edge of ZnO.

The electron injection of the three systems, P1/ZnO, (P1+Li^+)/ZnO, and (P1+MP)/ZnO, has been theoretically assessed using a simple approach, that is, by analyzing the corresponding one-electron-reduced systems. Such an approach is analogous to experimental spectro-electrochemical studies aimed at mimicking excited states resulting from photoinduced electron-transfer processes such as charge-separated or even (long-range) charge-transfer states.[46−48] Besides, this approach has been recently shown to be particularly suitable for predicting electron injection.[36]

The analysis of the electronic structure of the reduced systems is performed by computing their spin density maps, corresponding to the difference between α-spin and β-spin electron densities. The computed spin densities are reported in Figure 4 for the three systems. It appears that, for the three systems, the spin densities are delocalized over both the dye and the ZnO surface. Integration of the spin density located at the surface gives the proportion of injected electrons (Table 1). In the first system, without additive molecules in the electrolyte, the proportion of injected electrons is 18%. With adsorbed Li^+, the computed injection increases to 43%. Finally, in presence of MP, a reduction of the injection is calculated, dropping to 9%. Consequently, lithium ions must be added to the electrolyte when a better injection is sought in order to achieve higher efficiency.

To summarize, the overall picture we get from our theoretical investigations is the following. The dye P1 should exhibit an intense absorption band around 450 nm of pronounced charge-transfer character. Electron injection from the photoexcited dye into the CB of ZnO should be moderately efficient, but addition of lithium cations in the electrolyte is expected to dramatically increase the injection rate. In contrast, a reduction of the injection is anticipated when TBP is added to the electrolyte.

Experimental Validation. The absorption spectrum of the dye P1 in ethanol is presented in the Figure 1. The lower-energy band, centered at 453 nm, displays a high molar extinction coefficient (1.6×10^4 $M^{-1}\cdot cm^{-1}$). This transition is the one involved in the photon-to-electron conversion within the DSSC device. These findings are in excellent agreement with the theoretical outcomes of TD-DFT concerning UV−vis electronic absorption of P1, further confirming the good accuracy of the level of theory applied here to model the isolated dye.

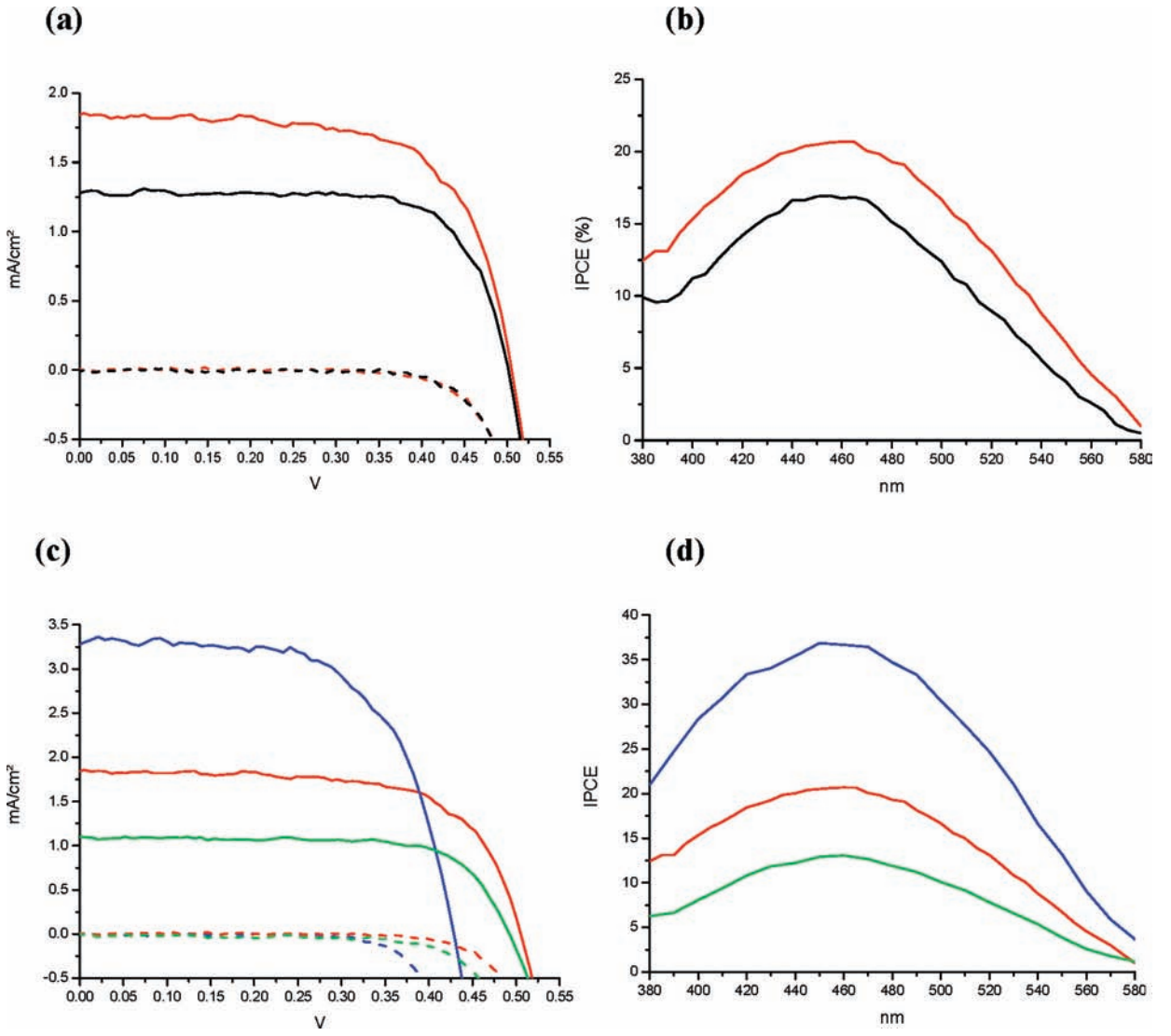

Figure 5. (a) $J-V$ and (b) IPCE curves measured for ZnO-based DSSCs sensitized by P1 without cholic acid (black) or with cholic acid (red) under AM1.5 illumination (full lines) and in the dark (dotted lines). $J-V$ (c) and IPCE (d) curves measured for ZnO-based DSSCs sensitized by P1 in presence of cholic acid using a standard electrolyte (red) or with Li^+ ion (blue) or TBP (green) added in the electrolyte.

The $J-V$ characteristics recorded under 1 sun irradiance for electrodeposited ZnO-based DSSCs sensitized with P1 are collected in Figure 5a, and cell performances are reported in Table 1. The influence of dyes' aggregation, well-known for DSSCs, was investigated by adding cholic acid to the dye solution during ZnO sensitization.[49] Indeed, aggregation can cause intermolecular energy transfer between dyes, thereby quenching the excited state before electron injection occurs.[22] Clearly, cholic acid increases the performance of the cell by almost 20%, due to an increase of the short-circuit current (J_{sc}) while the fill factor (FF) and the V_{oc} are kept nearly constant. This result suggests that dye molecules are probably aggregated on the ZnO surface. This is confirmed by the analysis of UV−vis spectra of the adsorbed dye in the presence or absence of cholic acid (Figure S5). A blue-shift of the low-energy absorption band of the adsorbed dye on ZnO (from 467 to 451 nm) is indeed observed upon addition of cholic acid, which is consistent with the destruction of J-type aggregates.[22,50] The low V_{oc} obtained (about 0.5 V) is probably a consequence of the use of a cationic dye, as was recently reported.[13,51] This phenomenon was explained by a decrease of the energy of the CB bottom edge of the semiconductor due to the orientation of the dipole moment of the cationic dye adsorbed on the surface.[51]

Theoretical calculations predicted that the presence of Li^+ should increase the rate of electron injection to the dye and consequently the photocurrent.

This phenomenon was also investigated at the experimental level. Photovoltaic characteristics ($J-V$ and IPCE curves) of DSSCs based on ZnO photosensitized with P1, using Li^+ and TBP additives, are depicted in Figure 5c,d. Cells' performances are summarized in Table 1. For comparison purposes, the same curves obtained with the standard electrolyte (i.e., without additives) are included in these figures. In presence of lithium, J_{sc} is increased but V_{oc} is decreased. This is the predicted behavior, since lithium adsorption lowers the energy of the CB bottom edge (so reducing the V_{oc}) but increases the rate of electron injection due to better energy matching of the LUMO/CB edge (so increasing the J_{sc}). The global power conversion

efficiency (η) of the P1/ZnO native system (ca. 0.6%) is then upgraded to 0.9% in the case of the (P1+Li^+)/ZnO optimized system. In contrast, addition of TBP in the electrolyte decreases J_{sc} while keeping V_{oc} almost constant. The observed decrease of J_{sc} is ascribed to the reduced efficiency of electron injection, in line with computational findings. Nevertheless, V_{oc} is not increased, which was also the expected behavior. This can be explained by the low injection efficiency, which may cause a lowering of the electronic density inside ZnO, to which the V_{oc} is also related.[22] The fact that the measured V_{oc} remains unchanged most likely indicates that the effect of electronic density lowering is compensated by the energy rise of the CB bottom edge. It is also worth noting that the TBP additive also increases the FF of the cell, which is a consequence of the ability of this molecule to quench the recombination process between the injected electron and the tri-iodide ion.[52] For this (P1+TBP)/ZnO system, the overall efficiency is reduced to 0.4%. Finally, the variation of IPCE curves as a function of the nature of additive molecules is in good agreement with the explanations proposed from the computed spin densities (Figure 5d).

CONCLUSION

In the present work, the suitability of a dye prototype based on a fused polycyclic expanded pyridinium to generate photocurrents in DSSC devices was assessed with a purposely conceived computational protocol. Theoretical outcomes were subsequently checked against experimental findings. Thus, the relevance of this computational approach has been validated, paving the way toward *in silico* screening and design of new dyes, moreover taking into account their actual environment for DSSC applications and cell optimization. This method is comprised of the following three steps:

(1) Calculation of the properties of the isolated dyes in order to get insights into their key intrinsic electronic features, including (i) UV−vis spectra, (ii) charge-transfer character of their lower-lying electronic transitions, and (iii) estimation of their excited-state oxidization potential.
(2) Calculation of the structural and electronic properties of the dye/semiconductor system using a periodic approach in order to access the electronic structure of the combined system.
(3) Calculation of the dye/semiconductor systems according to step (2) but in the presence of molecules composing the electrolyte, such as solvent or additives, that could modify their geometrical or electronic features. At this point, it is also possible to evaluate the electron injection efficiency in the presence of the different additive molecules.

Applied to the reference P1 molecule, this protocol gave interesting information. Molecular calculations provided an accurate estimation of UV−vis spectrum of the molecule. Clearly, taking into account the surface is essential for properly determining the relative position of the excited-state oxidation potential of the dye with respect to the CB bottom edge of the semiconductor. From this modeling, it appeared that the electronic configuration of the bare P1/ZnO system was not appropriate for DSSCs application. When the electrolyte composition was explicitly considered in the calculations (co-adsorption of additives), it was found that lithium ion should increase the electron injection of the dye, conversely to the TBP additive.

These results have been confirmed by the experimental $J-V$ and IPCE characteristics of DSSCs based on ZnO sensitized with P1. Theoretical insights allowed us to rationally improve the composition of the electrolyte by adding lithium ions and avoiding the use of the standard TBP additive. Thereby, the initial efficiency of 0.6% was increased to 0.9%.

This powerful theoretical approach should be used for the *in silico* optimization and design of both the dye and the electrolyte composition before carrying out time- and resources-consuming organic synthesis and cell construction.

ASSOCIATED CONTENT

Supporting Information. Details on water adsorption on ZnO, numbering scheme and optimized structure of P1, experimental and theoretical UV−vis spectrum of P1 with four ethanol molecules, geometrical parameters computed for P1 in solution and when adsorbed on ZnO, UV−vis spectra measured for P1 on ZnO in the absence or presence of cholic acid, complete ref 25, and characterization (^1H and ^{13}C NMR as well as ESI mass spectra) of P1. This material is available free of charge via the Internet at http://pubs.acs.org.

AUTHOR INFORMATION

Corresponding Author
ilaria-ciofini@chimie-paristech.fr; thierry-pauporte@chimie-paristech.fr; philippe.laine@univ-paris-diderot.fr

ACKNOWLEDGMENT

Prof. C. Adamo and Dr. J. Fortage are acknowledged for fruitful discussions. The French National Agency for Research (ANR) is acknowledged for financial support to I.C. and P.P.L. in the framework of the NEXUS project (Programme Blanc 2007, BLAN07-1-196405) and to T.P. and I.C. in the framework of the Asyscol project (Programme Habitat intelligent et solaire photovoltaïque 2008, ANR-08-HABISOL-002).

REFERENCES

(1) O'Regan, B.; Grätzel, M. *Nature* **1991**, *353*, 737.
(2) Hagfeldt, A.; Boschloo, G.; Sun, L.; Kloo, L.; Petterson, H. *Chem. Rev.* **2010**, *110*, 6595–6663.
(3) Ito, S.; Murakami, T. N.; Comte, P.; Liska, P.; Grätzel, C.; Nazeeruddin, M. K.; Grätzel, M. *Thin Solid Films* **2008**, *516*, 4613–4619.
(4) Yu, Q.; Wang, Y.; Yi, Z.; Zu, N.; Zhang, J.; Zhang, M.; Wang, P. *ACS Nano* **2010**, *4*, 6032–6038.
(5) Zeng, W.; Caot, Y.; Bai, Y.; Wang, Y.; Shi, Y.; Zhang, M.; Wang, F.; Pan, C.; Wang, P. *Chem. Mater.* **2010**, *22*, 1915–1925.
(6) Ramasamy, E.; Lee, J. *J. Phys. Chem. C.* **2010**, *114*, 22032–22037.
(7) Yoshida, T.; Zhang, J.; Komatsu, D.; Sawatani, S.; Minoura, H.; Pauporté, T.; Lincot, D.; Oekermann, T.; Schlettwein, D.; Tada, H.; Wöhrle, D.; Funabiki, K.; Matsui, M.; Miura, H.; Yanagi, H. *Adv. Funct. Mater.* **2009**, *19*, 17–43.
(8) Odobel, F.; Le Pleux, L.; Pellegrin, Y.; Blart, E. *Acc. Chem. Res.* **2010**, *43*, 1063–1071.
(9) Wang, Y.; Liu, Y.; Yang, H.; Wang, H.; Shen, H.; Li, M.; Yan, J. *Curr. Appl. Phys.* **2010**, *10*, 119–123.
(10) Zhang, W.; Zhang, D.; Fan, T.; Gu, J.; Ding, J.; Wang, H.; Guo, Q.; Ogawa, H. *Chem. Mater.* **2009**, *21*, 33–40.
(11) Guérin, V. M.; Magne, C.; Pauporté, Th.; Le Bahers, T.; Rathousky, J. *ACS Appl. Mater. Interfaces* **2010**, *2*, 3677–3685.
(12) Lupan, O.; Guérin, V. M.; Tiginyanu, I. M.; Ursaki, V. V.; Chow, L.; Heinrich, H.; Pauporté, T. *J. Photochem. Photobiol. A* **2010**, *211*, 65–73.

(13) Mishra, A.; Fischer, M. K. R.; Bäuerle, P. *Angew. Chem., Int. Ed.* **2009**, *48*, 2474–2499.
(14) Fortage, J.; Tuyèras, F.; Ochsenbein, P.; Puntoriero, F.; Nastasi, F.; Campagna, S.; Griveau, S.; Bedioui, F.; Ciofini, I.; Lainé, P. P. *Chem.—Eur. J.* **2010**, *16*, 11047–11063.
(15) Peltier, C.; Adamo, C.; Lainé, P. P.; Campagna, S.; Puntoriero, F.; Ciofini, I. *J. Phys. Chem. A* **2010**, *114*, 8434–8443.
(16) Fortage, J.; Peltier, C.; Nastasi, F.; Puntoriero, F.; Tuyèras, F.; Griveau, S.; Bedioui, F.; Adamo, C.; Ciofini, I.; Campagna, S.; Lainé, P. P. *J. Am. Chem. Soc.* **2010**, *132*, 16700–16713.
(17) Labat, F.; Ciofini, I.; Adamo, C. *J. Chem. Phys.* **2009**, *131*, 044708.
(18) Le Bahers, T.; Pauporté, Th.; Labat, F.; Lefèvre, G.; Ciofini, I. *Langmuir* 2011, *27*, 3442–3450.
(19) Nilsing, M.; Persson, P.; Ojamäe, L. *Chem. Phys. Lett.* **2005**, *415*, 375–380.
(20) Zhang, Q.; Dandeneau, C. S.; Zhou, X.; Cao, G. *Adv. Mater.* **2009**, *21*, 4087–4108.
(21) Le Bahers, T.; Pauporté, T.; Scalmani, G.; Adamo, C.; Ciofini, I. *Phys. Chem. Chem. Phys.* **2009**, *11*, 11276–11284.
(22) Pastore, M.; De Angelis, P. *ACS Nano* **2010**, *4*, 556–562.
(23) Le Bahers, T.; Labat, F.; Pauporté, Th.; Ciofini, I. *Phys. Chem. Chem. Phys.* **2010**, *12*, 14710–14719.
(24) Jacquemin, D.; Perpete, E. A.; Ciofini, I.; Adamo, C. *Acc. Chem. Res.* **2009**, *42*, 326–334.
(25) Frisch, M. J.; *Gaussian 09*, Revision A.02; Gaussian, Inc.: Wallingford, CT, 2010.
(26) Adamo, C.; Barone, V. *J. Chem. Phys.* **1999**, *110*, 6158.
(27) Krishnan, R.; Binkley, J. S.; Pople, J. A. *J. Chem. Phys.* **1980**, *72*, 650–654.
(28) Tomasi, J.; Mennucci, B.; Cammi, R. *Chem. Rev.* **2005**, *105*, 2999–3094.
(29) Barone, V.; Cossi, M. *J. Phys. Chem. A* **1998**, *102*, 1995–2001.
(30) Saunders, V. R.; Dovesi, R.; Roetti, C.; Orlando, R.; Zicovich-Wilson, C. M.; Harrison, N. M.; Doll, K.; Civalleri, B.; Bush, I.; D'Arco, Ph.; Llunell, M. *Crystal 09 User's Manual*; Universita di Torino: Torino, Italy, 2009.
(31) Wöll, C. *Prog. Surf. Sci.* **2007**, *82*, 55–120.
(32) The basis set can be dowloaded at http://www.crystal.unito.it/Basis_Sets/Ptable.html.
(33) Barthelat, J.-C.; Durand, P. *Gazz. Chim. Ital.* **1978**, *108*, 225.
(34) Barthelat, J.-C.; Durand, P.; Serafini, A. *Mol. Phys.* **1977**, *33*, 159.
(35) Hay, P. J.; Wadt, W. R. *J. Chem. Phys.* **1985**, *82*, 284.
(36) Labat, F.; Ciofini, I; Hratchian, H.; Frisch, M.; Raghavachari, K.; Adamo, C. *J. Am. Chem. Soc.* **2009**, *131*, 14290–14298.
(37) Katritzky, A. R.; Zakaria, Z.; Lunt, E. *J. Chem. Soc., Perkin Trans. 1* **1980**, 1879–1887.
(38) Pauporté, T.; Rathousky, J. *J. Phys. Chem. C* **2007**, *111*, 7639–7644.
(39) Pauporté, T.; Yoshida, T.; Cortès, R.; Froment, M.; Lincot, D. *J. Phys. Chem. B* **2003**, *107*, 10077–10082.
(40) Peltier, C.; Lainé, P. P.; Scalmani, G.; Frisch, M. J.; Adamo, C.; Ciofini, I. *J. Mol. Struct. THEOCHEM* **2009**, *914*, 94–99.
(41) Goux, A.; Pauporté, Th.; Chivot, J.; Lincot, D. *Electrochim. Acta* **2005**, *50*, 2239–2248.
(42) De Angelis, F.; Armelao, L. *Phys. Chem. Chem. Phys.* **2010**, *13*, 467–475.
(43) Kopidakis, N.; Neale, N. R.; Frank, A. J. *J. Phys. Chem. B* **2006**, *110*, 12485–12489.
(44) Jennings, J. R.; Wang, Q. *J. Phys. Chem. C* **2010**, *114*, 1715–1724.
(45) Onicha, A. C.; Castellano, F. N. *J. Phys. Chem. C* **2010**, *114*, 6831–6840.
(46) Ciofini, I.; Lainé, P. P.; Bedioui, F.; Adamo, C. *J. Am. Chem. Soc.* **2004**, *126*, 10763–10777.
(47) Lainé, P. P.; Ciofini, I.; Ochsenbein, P.; Amouyal, E.; Adamo, C.; Bedioui, F. *Chem.—Eur. J.* **2005**, *11*, 3711–3727.
(48) Lainé, P. P.; Loiseau, F.; Campagna, S.; Ciofini, I.; Adamo, C. *Inorg. Chem.* **2006**, *45*, 5538–5551.
(49) Sakuragi, Y.; Wang, X.-F.; Miura, H.; Matsui, M.; Yoshida, T. *J. Photochem. Photobiol. A* **2010**, *216*, 1–7.
(50) Peyratout, C.; Donath, E.; Daehne, L. *J. Photochem. Photobiol. A* **2001**, *142*, 51–57.
(51) Liang, Y.; Cheng, F.; Liang, J.; Chen, J. *J. Phys. Chem. C* **2010**, *114*, 15842–15848.
(52) Boschloo, G.; Häggman, L.; Hagfeldt, A. *J. Phys. Chem. B* **2006**, *110*, 13144–13150.